

14 MHz rate photon counting with room temperature InGaAs/InP avalanche photodiodes

PAUL L. VOSS, KAHRAMAN G. KÖPRÜLÜ,
SANG-KYUNG CHOI†, SARAH DUGAN and PREM KUMAR

Center for Photonic Communication and Computing,
ECE Department, Northwestern University,
2145 Sheridan Road, Evanston, IL 60208-3118, USA

†Time and Frequency Group, Korea Research Institute of Standards
and Science, P.O. Box 102, Yuseong, Daejeon 305-600, Korea

(Received 11 August 2003)

Abstract. We have developed high speed gated-mode single-photon counters based on InGaAs/InP avalanche photodiodes for use at 1.55 μm wavelength. Operation at room temperature allows afterpulse probability to be below 0.2% for gate rates up to 14 MHz. We obtained optimum noise-equivalent power of $2.2 \times 10^{-15} \text{ W Hz}^{-1/2}$ at 14% quantum efficiency with dark-count probability of 0.2%. We propose a metric (noise-equivalent power divided by gate frequency) for comparing high speed photon counters and show that for this metric our system outperforms previously reported counters at 1.55 μm wavelength. We demonstrate that for gate widths of a nanosecond or below, the differing amplitude distributions of dark versus light counts allow an optimal decision threshold to be set for a given bias voltage.

1. Introduction

Recent theoretical and experimental developments have generated interest in applications such as quantum cryptography [1], linear-optics quantum computation [2] and ultra-sensitive time-domain reflectometry [3]. A key enabling element of these technologies is the ability to count single photons in an efficient manner. Of particular interest are improvements in single-photon counters at 1.3 and 1.55 μm wavelengths, where the characteristics of silica optical fibres allow for low-loss transmission of photons over long distances. Currently available single-photon detectors at these wavelengths suffer from several drawbacks. The first of these is imperfect quantum efficiency which can be close to unity at the above wavelengths for conventional high light-level measurements with PIN or avalanche photodiodes. In addition, following a detection event, some dead time is usually required for resetting the detector. If the detector is opened at too high a rate, there is the possibility of afterpulsing, where residual charge carriers from the previous detection event cause a false detection count. Most detectors also suffer from some dark counts where thermally excited charge carriers cause a false detection event. Another drawback is that most detectors cannot distinguish the number of arriving photons. With the available detectors, one must make trade-offs in the above requirements to obtain satisfactory performance for a particular application.

Avalanche photodiodes (APDs) are capable of detecting single photons when reverse biased above the breakdown voltage [4]. When a single photon is absorbed, the generated electron and/or hole can initiate a detectable avalanche. If the reverse bias remains above the breakdown voltage, the p–n junction breaks down and the avalanche current is limited by the ohmic resistance of the diode. There are three possibilities for arming and resetting the APD. One may use passive quenching, wherein a large resistor is placed in series with the APD. The avalanche current flowing through this resistor causes the voltage across the APD to drop below the breakdown voltage. The avalanche subsides and the bias voltage recovers exponentially according to the RC time constant of the circuit, where R is the resistance in series with the APD and C is the capacitance of the APD. This RC time constant is chosen large enough for afterpulsing to remain acceptably small. One may also use active quenching, wherein an electronic circuit detects and takes action to quench the avalanche before rearming the APD after a suitable delay. The third method, which is used in this paper, operates the APD in a gated mode (or Geiger mode), wherein the APD is activated and deactivated by the leading and trailing edges of an applied gate pulse that briefly biases the diode above breakdown. This method allows for the best suppression of dark counts, and is preferred when detecting photons arriving in short optical pulses.

To date, the best practical counters at visible wavelengths have been constructed using silicon APDs. The best commercially available photon-counting modules (PCMs), made by Perkin–Elmer (Model SPCM-AQR-16), formerly made by EG&G, have 50–70% quantum efficiency near 630 nm wavelength, <25 dark counts per second, and can count at rates of 10–15 Megacounts s⁻¹ [5]. The silicon APDs work well because of both the material system's suitability for the task and the availability of silicon of nearly perfect quality. The dark-count rate is low enough for the PCMs to be operated in the active-quench mode. However, the quantum efficiency of silicon drops off significantly for wavelengths greater than 1 μm (the silicon PCM has efficiency of 2% at 1 μm). Although materials with high absorption efficiency further in the infrared are available, obtaining low-noise avalanche gain is problematic. The use of APDs with InGaAs as the absorption region separate from a multiplication layer of InP has proven to be a better solution [6–13] than germanium APDs [14, 15]. However, the dark-count rates in these devices are very large in comparison to the silicon devices even when the APDs are cooled. The reported quantum efficiencies are typically between 10 to 40% and the APDs are typically operated at a count rate of 100 kHz in order to keep the afterpulsing rate acceptably low. After a detection event, the afterpulsing probability in such devices is relatively high because of the trapping centres that are formed at the interface between the InGaAs and InP layers.

In this paper we report on the characteristics of two InGaAs/InP-based photon counters that we assembled using APDs manufactured by JDS Uniphase (Model EPM239BA). These fibre-pigtailed APDs have a measured responsivity of $0.55 \pm 0.02 \text{ A W}^{-1}$ at an inferred avalanche gain of 1 when operated in the linear mode. In section 2 we present the design of our set-up. In section 3 we report the results of quantum efficiency versus dark-count probability measurements. In section 4 we discuss our characterization of the afterpulses. In section 5 we propose a metric for comparing high-speed photon counters and compare our results against others reported to date at 1.55 μm wavelength. In section 6 we present our conclusions.

2. Experimental configuration

A gated-mode photon counter must synchronize electrical gate pulses precisely with incoming optical pulses. This is usually done when working with pulses from a mode-locked laser by recovering the optical clock and tuning an electronic delay in the electrical path. Our experiment uses a passively mode-locked fibre laser producing ~ 8 ps optical pulses at 14.13 MHz rate. Approximately 50% of the fibre-laser output is used for recovery of the 14 MHz optical clock, another 40% is detected with PIN photodiodes of 1 GHz bandwidth to monitor the timing stability, and the remaining 10% is further attenuated for use as the single-photon-level input to the photon counters. A schematic of the clock-recovery and programmable electronic-delay circuits is provided in figure 1. Clock recovery is done with a fibre-connectorized InGaAs photodiode (Perkin-Elmer, Model C30618BFC) followed by a 20 dB signal-gain amplifier based on an op-amp (Analog Devices, Model 8009). The amplified photocurrent is then filtered with a 22 MHz low-pass filter to obtain a clean sine wave for use by the delay line, which is based on a 180° phase shifter (Minicircuits, Model SPH-16). The electronic delay is set by a variable voltage between 0.5 to 5 V, which is applied to the phase shifter by a computer controlled D/A board (National Instruments, Model PCI8611). In order to suppress harmonics generated in the phase shifter and to block the dc voltage, the output of the phase shifter is filtered by a bandpass filter centred at 14 MHz. To provide a high slope on the rising edge of the 14 MHz phase-shifted signal, that signal is amplified with a linear gain of 4 by an AD8009

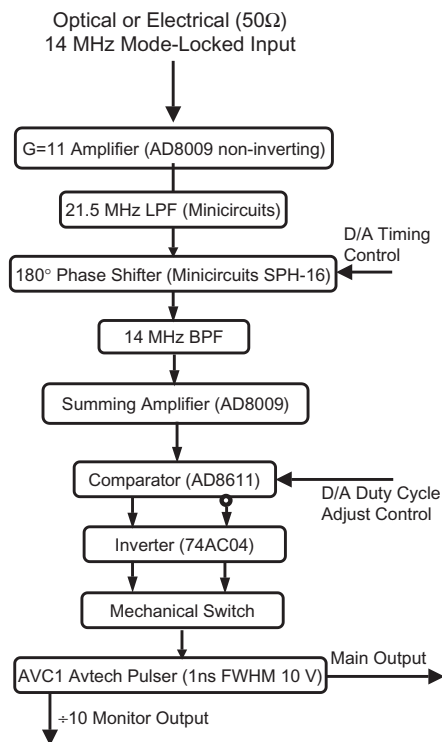


Figure 1. Schematic of the delay-line circuit.

op-amp, which is configured as an adder so that the phase-shifted signal has a bias of 0.75 V. The adder output enters a comparator (Analog Devices, Model AD8611) with complementary outputs that provide square pulses. By adjusting the other input to the comparator with a computer controlled D/A signal we obtain output pulses with a 50% duty cycle. The outputs are buffered by NOT gates (74AC04) and one of them is selected with a mechanical switch, thus providing a 180° phase shift. The selected output serves as a trigger for the pulse generator (Avtech, Model AVM-2-C), which is most stable when triggered with a 50% duty cycle clock. The total measured timing jitter on time scales less than a few seconds of the pulse-generator output is less than 50 ps, but there is a slow drift of the timing within a range of ± 100 ps which occurs over the course of several seconds. This slow drift is due to the phase shifter and can be improved with the use of a higher quality part.

The detection and thresholding part of the photon-counting system is shown in figure 2. For the data reported in this paper, unless otherwise specified, we choose pulses of 10 V in amplitude and 800 ps FWHM. Pulses of a longer duration cause more dark counts, while shorter duration pulses increase the system's sensitivity to timing drift. These 800 ps pulses pass through a simple bias tee composed of a pass-through capacitor for the pulses and an inductor through which the dc voltage is applied. Approximately 1% of each electrical pulse leaks through the junction capacitance of the diode, causing a deterministic 'ringing' that occurs identically for each pulse. Most of the energy in the 'ringing' is concentrated above frequencies of 1 GHz. This 'ringing' pulse and any avalanche photocurrent present is then amplified with a linear gain of 10 and 3 dB bandwidth of 100 MHz. The filtered 'ringing' plus the avalanche photocurrent is sampled by a 12 bit analog-to-digital (A/D) converter (Analog Devices, Model AD9433), whose resolution is about 0.5 mV. The A/D converter is triggered by the amplified, monitor output from the pulse generator. The digitally sampled output then enters a digital comparator circuit, whose threshold is set to values supplied via the parallel port of a controlling personal computer (PC). Threshold values are loaded into three cascaded serial-to-parallel chips (74AC283) in two's complement format. The parallel outputs then enter the inputs of three cascaded 4 bit adders (74AC164).

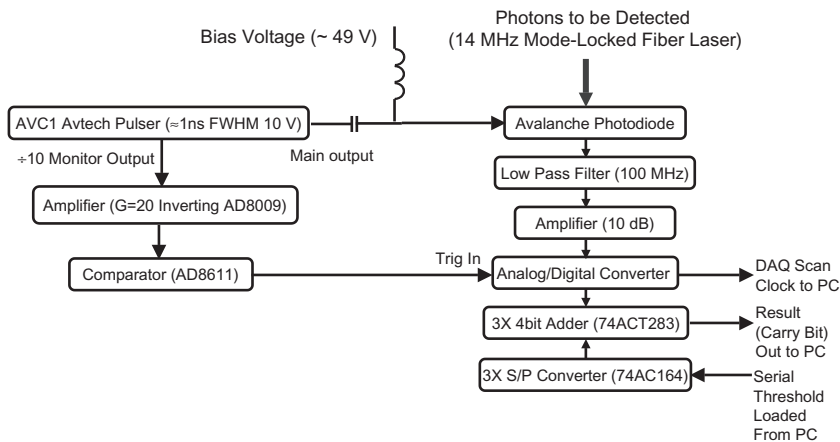


Figure 2. Schematic of the detection and thresholding set-up.

The other inputs to the adder come from the A/D outputs. The carry-out bit from the third adder signals whether the A/D value exceeded the digitally set threshold or not, allowing one to decide whether a detection event occurred or not. A personal-computer-interface (PCI) card (National Instruments, Model NI5102) in the PC, which is clocked by the data-ready output from the A/D converter, acquires the carry-out bit for each gate pulse.

3. Quantum efficiency and dark count

The amplitude distributions of the output of APD A were measured with a sampling oscilloscope (Lecroy, Model LT354) after being amplified by a linear gain of 10. These distributions are shown in figure 3 as persistence traces when 50 V bias and 800 ps wide gate pulses of 10 V amplitude were applied. One can clearly see the difference in amplitude between (a) no avalanches with the light blocked and bias voltage lowered, (b) dark counts with the light blocked but the bias voltage and gate pulses on, and (c) 'light plus dark' counts with the light unblocked and approximately 1 photon per pulse entering the APD. We zoom in on a particular point on the time axis, where the voltage due to avalanches maximally exceeds the leakage voltage, and show the results as pulse-height histograms in figure 4. The histograms of the 'light plus dark' counts and the dark counts were computed from 2 million samples each for the case of 49 V bias

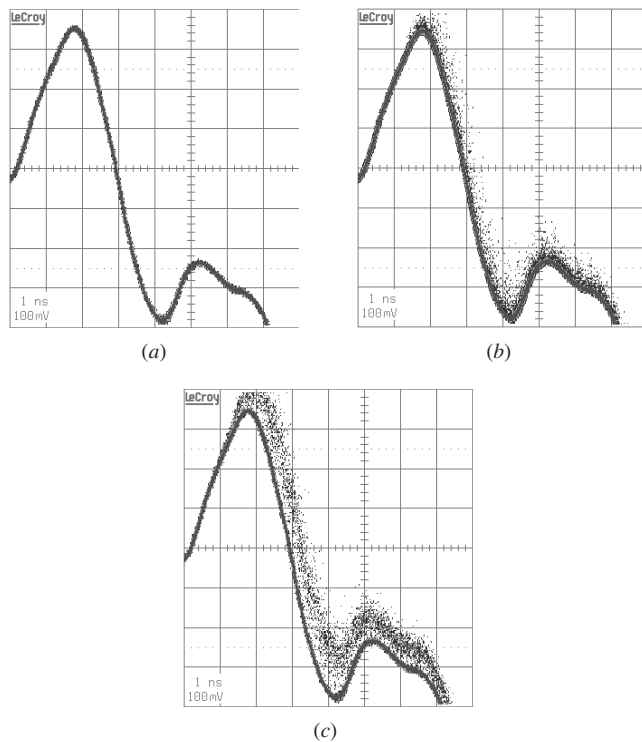


Figure 3. Persistence traces obtained with a sampling oscilloscope having a 1 Gs s^{-1} sampler. (a) Filtered and amplified 'ringing' at 47 V bias. (b) Dark count persistence at 50 V bias. (c) Light count persistence at 50 V bias. Horizontal scale is 1 ns div^{-1} .

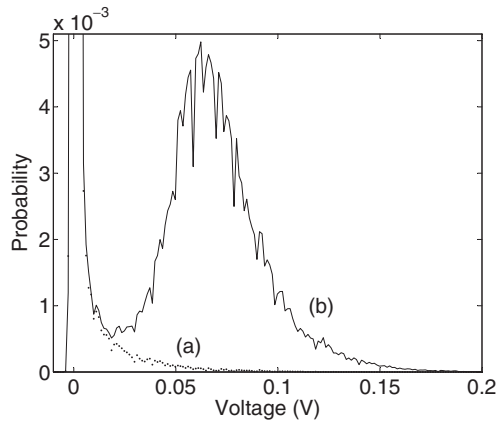


Figure 4. Output-voltage histogram of (a) dark counts and (b) 'light plus dark' counts (solid line). The APD output is filtered and amplified by 10. Bias voltage is 49 V.

and 10 V gate pulses of 1 ns FWHM. Approximately one photon per pulse entered the APD during the 'light plus dark' distribution measurement. Because for most gate pulses no avalanche occurs, the histograms are peaked near zero volts for both the 'light plus dark' and the dark measurements. This zero peak has been cut off in figure 4 to provide the necessary resolution for the avalanche amplitude histograms. The jaggedness seen in the histograms is due to the unequal bin width of the 8 bit A/D converter in the sampling oscilloscope.

Because there are many more light counts than dark counts in the measured 'light plus dark' distribution, the light counts have essentially the same distribution. Differing pulse-height distributions for light counts and dark counts do not occur for long gate pulses, because the avalanche photocurrent saturates on a nanosecond time scale to produce the same output voltage for both light and dark counts. When using one nanosecond or shorter gate pulses, the avalanches due to the dark events start at random times and thus usually do not last the full gate width to produce much current before the gate closes. The light events, on the other hand, start at approximately the same time (owing to the pulsed nature of the incident light), which is optimized to produce the most avalanche current. In the above, we assume that the light and dark counts have the same spatial distribution in the InGaAs/InP material, which may not be the case. If the dark events tend to occur where they see less total avalanche gain than that seen by the light events, the two would be partially distinguishable for this reason as well.

In order to measure the quantum efficiency of both APDs, we attenuate the incoming picosecond pulses from the fibre laser so that on average $M = 1.0 \pm 0.023$ photons per pulse enter the fibre that is pigtailed to the APDs. For pulsed-light arriving at a repetition rate of 14 MHz and a wavelength of 1537 nm, a mean of one photon per pulse corresponds to -87.4 dBm of optical power. This attenuation adjustment is done with a calibrated variable attenuator (JDSU, Model HA9). When light impinges on the detectors, we measure the 'light + dark' count probability per pulse $P_{L+D}(1)$ and when the light is blocked, we measure the dark-count probability per pulse $P_D(1)$. We assume that the dark events are Poisson distributed and the chance of two or more dark avalanches occurring for a single gate pulse is negligibly small. Also using the fact that

the probability $P(0)$ of no photons being detected for a single gate pulse is $P(0) = \exp(-\eta M)$ for Poisson-distributed input laser light, where η is the detection quantum efficiency, we use

$$\eta = -\ln \left[1 - \frac{P_{L+D}(1) - P_D(1)}{1 - P_D(1)} \right] / M \tag{1}$$

to obtain the quantum efficiency. The measured results of quantum efficiency versus dark-count probability for the two tested APDs are shown in figures 5 and 6, respectively, for various bias voltages. The data was obtained by scanning the digital threshold while keeping the applied gate-pulse height and width fixed at 12 V and 800 ps, respectively. In figure 5, we show the results for APD A for which the bias voltage was stepped in one-volt increments from 49 to 53 V. In figure 6 we show the results for APD B for bias voltages from 48 to 52 V. In figure 7, plots of quantum efficiency versus dark-count probability are shown, which result when the threshold is held constant, but the bias voltage is scanned for the same gate-pulse height and width as in figures 5 and 6. The bias was scanned for APD A from 48.8 to 51.2 V and for APD B from 49.4 to 51.0 V in 200 mV increments.

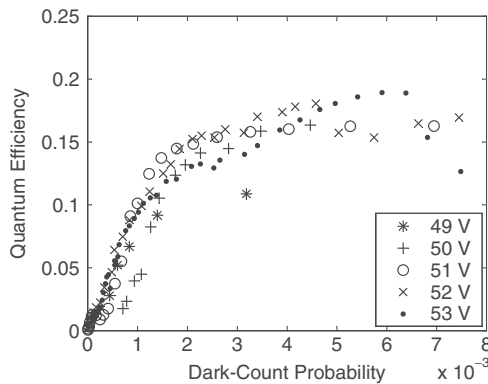


Figure 5. APD A: quantum efficiency versus dark-count probability as threshold is scanned.

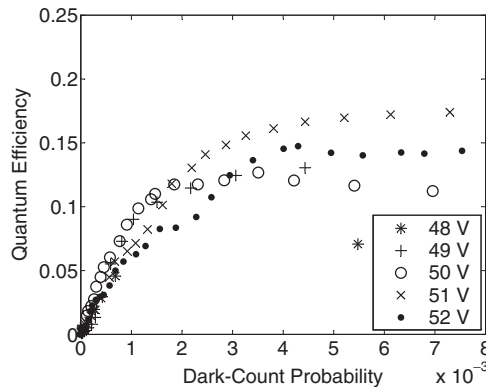


Figure 6. APD B: quantum efficiency versus dark-count probability as threshold is scanned.

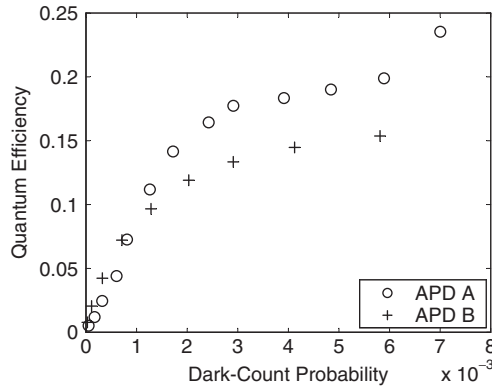


Figure 7. Quantum efficiency versus dark-count probability for APD A (\circ) and APD B ($+$) as the bias voltage is scanned in 200 mV increments. APD A is scanned from 48.8 to 51.2 V and APD B is scanned from 49.4 to 51.0 V.

Comparing figures 5, 6 and 7, we see that very similar results are obtained either by scanning the threshold or the bias voltage.

The similar shape of the data in each of these figures is best explained by considering the unequal amplitude histograms of the light versus dark avalanches in figure 4. As either the decision threshold is lowered or the bias voltage is increased, the increasing detection of a relatively larger proportion of the light counts compared to the dark counts gives the steep slope observed below a dark-count probability of about 0.2%. Further decrease of the decision threshold with concomitant increase in the dark-count probability leads to a relatively smaller proportion of the light counts being detected compared to the dark counts. Beyond the dark-count probability of 0.2%, the decreasing contribution of the light counts gives the almost flat slope in figures 5–7 as either the bias voltage is further increased or the decision threshold is further lowered.

4. Afterpulses

We characterize afterpulsing at different gate repetition rates and at different bias voltages. It has been previously noted [6] for gated-mode operation of APDs that higher bias voltages increase the afterpulsing rate for a given gate rate. The further the APD is above breakdown, the larger is the avalanche size, thus filling more trapping centres, which take longer to completely empty. We measure the afterpulsing probability for APD A at bias voltages of 50, 51 and 52 V for gate frequencies from 4 to 20 MHz. In previously published work on gated-mode APDs [6, 7], afterpulsing probability has been measured by impinging a multi-photon light pulse on the APD during one gate pulse, thus ensuring an avalanche occurs during that gate, and then measuring the probability of an avalanche occurring during the following gate pulse with no input light. This is an accurate method in those experiments because the afterpulse probability is at least an order of magnitude greater than the dark-count probability. This method would be inaccurate for our set-up because at high rates and at room temperature the afterpulse probability and the dark-count probability are of the same order. With our set-up, however, it is still possible to measure a difference between the

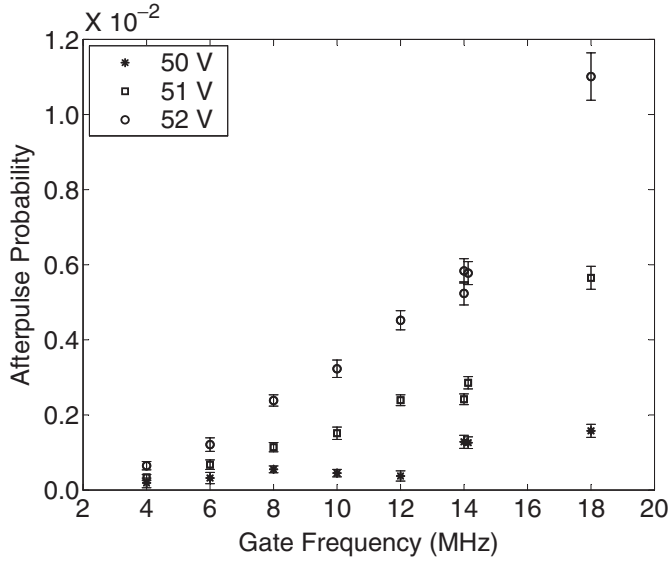


Figure 8. Afterpulse probability versus the gate frequency: *, 50 V; \square , 51 V; \circ , 52 V. Error bars calculated from the standard deviation of 10 batches of 100 million gate pulses.

probability of a count occurring and the probability for a count to occur during a gate pulse conditioned on the occurrence of a count in the previous gate pulse, $P_n(1|P_{n-1} = 1)$. The excess afterpulse probability, which we refer to as the afterpulse probability in the rest of this paper, is then $P_n(1|P_{n-1} = 1) - P(1)$. In order to simplify the experiment, we choose to measure the afterpulse probability with no light impinging on the APD. If the detection threshold for each bias voltage is set such that $P_D(1) = 0.001$, then we count only those dark events that produce more avalanche current than the mean avalanche current produced by a light count (see figures 4–6). By doing so, we acquire afterpulse data under conditions slightly more severe than those occurring when single-photon-level light impinges on the APD.

The results for such measurements are shown in figure 8. We acquire measurements in 10 batches of $N_{tc} = 100$ million gate pulses, from which we obtain $P_n(1|P_{n-1} = 1)$ and $P_D(1)$. Thus in each batch, we acquire approximately $N_{dc} = 10^5$ dark counts and roughly $N_{ap} = 100$ to 1000 afterpulse counts. The afterpulse rate is then given by $(N_{ap}/N_{dc}) - (N_{dc}/N_{tc})$. The error bars in the plots in figure 8 are obtained by calculating the standard deviation of the results from the 10 batches. It is important to note that above 14 MHz, it is difficult to obtain reliable results, even though the results at 14 MHz and at lower rates are reproducible. It is not clear if this is caused by the properties of the APD or of the detection electronics. Also, at 50 V the data seem to follow a smooth curve to a lesser degree than the results at 51 and 52 V. One reason for this behaviour is that the measured dark-count probability exhibits fluctuations beyond the statistically expected fluctuations. This is perhaps due to long-term drift in the amplitude or width of the applied gate pulses. Such fluctuation in the dark-count probability makes it harder to measure the afterpulse rate because we end up subtracting two close-to-equal probability estimates with relatively large uncertainties in them.

Nevertheless, as expected, the afterpulse probability decreases for weaker avalanches which occur at lower bias voltages. At our maximum operation rate of 14 MHz, and for the threshold set to obtain good quantum efficiency, we get the best result of 0.2% afterpulse probability at a bias of 50 V. We expect to further improve the system with regards to the afterpulse probability by increasing the external amplification of the avalanche photocurrent and lowering the bias voltage. By doing so the avalanche current from the APD would be smaller, but after increased electronic amplification, would enter the A/D circuit with the same size. It should be noted that in this regime the afterpulse probability would be smaller than the dark-count probability, and would be quite difficult to measure accurately. With such improvement, however, the effect of afterpulses would be negligible.

5. A metric for high-speed photon counters

InGaAs/InP APD-based photon counters operating at room temperature suffer from higher dark-count rate, and thus have higher noise-equivalent power than those based on cooled APDs. Despite this, room-temperature operation may be useful in applications where only average values need to be obtained quickly, or where coding may be used to overcome the lower signal-to-noise ratio. Applications such as long distance optical time-domain reflectometry require some sort of averaging in order to provide estimates of reflection coefficients. In addition, in many laboratory situations, it is advantageous to take measurements as rapidly as possible. Thus higher-rate counting is an enabling technology. Therefore, a suitable metric for comparing fast photon-counting systems would be the noise-equivalent power (NEP) divided by the gate frequency (NEP/ f), which should be as low as possible. NEP is written as $h\nu(2R)^{1/2}/\eta$ (W Hz^{-1/2}), where $h = 6.626 \times 10^{-34}$ J s is the Planck constant, ν is the optical frequency, R is the dark-count rate for one second of turn-on time and η is the quantum efficiency of the detector. In the gated mode, the dark-count probability must be multiplied by the inverse of the gate width in seconds to obtain R . NEP/ f then has units of W Hz^{-3/2}. We have estimated NEP/ f for our set-up as well as for several other published experiments and commercially available photon-counting systems. By this metric, we outperform other InGaAs/InP photon counters as shown in table 1.

Table 1. Comparison of NEP/ f for various single-photon counters operating at 1.55 μ m wavelength. For comparison with the best performance available at visible wavelengths, we also include the silicon-APD-based Perkin-Elmer [5] SPCM-AQR-16 in this table.

Reference	APD	Temp	NEP	Rate	NEP/Rate
Perkin-Elmer [5]	SPCM-AQR-16	cooled	2.7×10^{-18}	15 MHz	1.8×10^{-25}
This paper	EPM239BA	293 K	2.2×10^{-15}	14.1 MHz	1.6×10^{-22}
Fiorentino <i>et al.</i> [12]	EPM239BA	293 K	1.0×10^{-15}	588 kHz	1.7×10^{-21}
Tomita and Nakamura [11]	EPM239BA	178 K	1.6×10^{-15}	100 kHz	1.6×10^{-20}
Namekata <i>et al.</i> [10]	EPM239BA	218 K	2.1×10^{-16}	10 kHz	2.1×10^{-20}
Ribordy <i>et al.</i> [6]	FPD5W1KS	200 K	5.0×10^{-16}	10 kHz	4.7×10^{-20}
Hiskett <i>et al.</i> [8]	FPD13U8UR	77 K	4×10^{-16}	1 kHz	4×10^{-19}

Note the very large advantage commercially available silicon visible-photon counters hold over the recently reported infrared photon counters.

6. Conclusion

In conclusion, there are several applications for high-rate photon counting at 1.55 μm . We have defined a metric (NEP/ f) to compare different high-rate photon counting set-ups. To the best of our knowledge, for this metric our set-up outperforms previously published work at 1.55 μm . We report optimum noise-equivalent power of $2.2 \times 10^{-15} \text{ W Hz}^{-1/2}$ at a quantum efficiency of 14% with dark-count probability less than 0.2%.

Acknowledgments

This work was supported by the US Office of Naval Research under Grant No. N00014-03-1-0179 and by the US Army Research Office, under a MURI grant DAAD19-00-1-0177.

References

- [1] GISIN, N., RIBORDY, G., TITTEL, W., and ZBINDEN, H., 2002, *Rev. Mod. Phys.*, **74**, 145, and references therein.
- [2] KNILL, E., LAFLAMME, R., and MILBURN, G. J., 2001, *Nature*, **409**, 46.
- [3] GARSIDE, B. K., and PARK, R. E., 1990, *Fiber Optic and Laser Sensors VII, Proceedings of the SPIE*, Vol. 1169, edited by R. P. DePaula and E. Udd (Bellingham, WA: SPIE), p. 89.
- [4] OLDHAM, W. G., SAMUELSON, R. R., and ANTOGNETTI, P., 1972, *IEEE Trans. Electron. Dev.*, **ED-19**, 1056.
- [5] <http://optoelectronics.perkinelmer.com/content/Datasheets/SPCM-AQR.pdf>.
- [6] RIBORDY, G., GAUTIER, J. D., ZBINDEN, H., and GISIN, N., 1998, *Appl. Optics*, **37**, 2272.
- [7] LACAITA, A., ZAPPA, F., COVA, S., and LOVATI, P., 1996, *Appl. Optics*, **35**, 2986.
- [8] HISKETT, P. A., BULLER, G. S., LOUDON, A. Y., SMITH, J. M., GONTIJO, I., WALKER, A. C., TOWNSEND, P. D., and ROBERTSON, M. J., 2000, *Appl. Optics*, **39**, 6818.
- [9] RARITY, J. G., WALL, T. E., RIDLEY, K. D., OWENS, P. C. M., and TAPSTER, P. R., 2000, *Appl. Optics*, **39**, 6746.
- [10] NAMEKATA, N., MAKINO, Y., and INOUE, S., 2002, *Opt. Lett.*, **27**, 954.
- [11] TOMITA, A., and NAKAMURA, K., 2002, *Opt. Lett.*, **27**, 1827.
- [12] FIORENTINO, M., VOSS, P. L., SHARPING, J. E., and KUMAR, P., 2002, *IEEE Photon. Technol. Lett.*, **14**, 983.
- [13] BETHUNE, D. S., and RISK, W. P., 2000, *IEEE J. Quantum Electron.*, **36**, 340.
- [14] LACAITA, A., FRANCESE, P. A., ZAPPA, F., and COVA, S., 1994, *Appl. Optics*, **33**, 6902.
- [15] OWENS, P. C. M., RARITY, J. G., TAPSTER, P. R., KNIGHT, D., and TOWNSEND, P. D., 1994, *Appl. Optics*, **33**, 6895.